Ligand-based design identifies a potent NUPR1 inhibitor exerting anticancer activity via necroptosis

Patricia Santofimia-Castaño, Yi Xia, Wenjun Lan, Zhengwei Zhou, Can Huang, Ling Peng, Philippe Soubeyran, Adrián Velázquez-Campoy, Olga Abián, Bruno Rizzuti, et al.

JCI The Journal of Clinical Investigation

Ligand-based design identifies a potent NUPR1 inhibitor exerting anticancer activity via necroptosis

Patricia Santofimia-Castaño, … , Jose L. Neira, Juan Iovanna

J Clin Invest. 2019. https://doi.org/10.1172/JCI127223.

Research In-Press Preview Gastroenterology Oncology

Graphical abstract

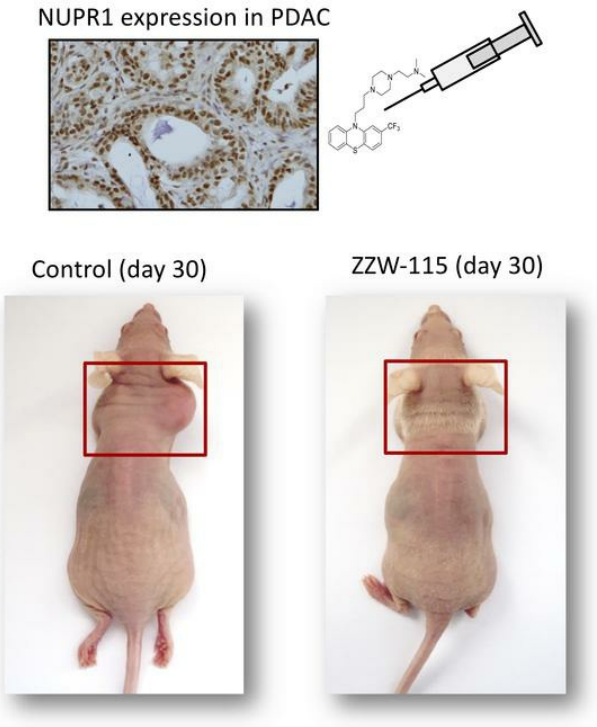

Ligand-based design identifies a potent NUPR1 inhibitor exerting anticancer activity via necroptosis

Patricia Santofimia-Castaño[1,#], Yi Xia[2,#], Wenjun Lan[1, 3,#], Zhengwei Zhou[2], Can Huang[1], Ling Peng[3], Philippe Soubeyran[1], Adrián Velázquez-Campoy[4,5], Olga Abián[4,6], Bruno Rizzuti[7], José L Neira[8]*, Juan Iovanna[1]*

[1]Centre de Recherche en Cancérologie de Marseille (CRCM), INSERM U1068, CNRS UMR 7258, Aix-Marseille Université and Institut Paoli-Calmettes, Parc Scientifique et Technologique de Luminy, 163 Avenue de Luminy, 13288 Marseille, France.

[2]Chongqing Key Laboratory of Natural Product Synthesis and Drug Research, School of Pharmaceutical Sciences, Chongqing University, No.55 Daxuecheng South Road, Chongqing 401331, P. R. China.

[3]Aix-Marseille Université, CNRS, Centre Interdisciplinaire de Nanoscience de Marseille, UMR 7325, «Equipe Labellisée Ligue Contre le Cancer», Parc Scientifique et Technologique de Luminy, 163 Avenue de Luminy, 13288 Marseille, France.

[4]Instituto de Biocomputación y Física de Sistemas Complejos, Joint Units IQFR-CSIC-BIFI, and GBsC-CSIC-BIFI, Universidad de Zaragoza, Spain; Instituto Aragonés de Ciencias de la Salud (IACS), Zaragoza, Spain; Aragon Institute for Health Research (IIS Aragon), Zaragoza, Spain; Centro de Investigación Biomédica en Red en el Área Temática de Enfermedades Hepáticas y Digestivas (CIBERehd), Barcelona, Spain; Departamento de Bioquímica y Biología Molecular y Celular, Universidad de Zaragoza, Zaragoza, Spain.

[5]Fundacion ARAID, Government of Aragon, Zaragoza, Spain

[6]Instituto Aragonés de Ciencias de la Salud (IACS), Zaragoza, Spain

[7]CNR-NANOTEC, Licryl-UOS Cosenza and CEMIF.Cal, Department of Physics, University of Calabria, Via P. Bucci, Cubo 31 C, 87036 Arcavacata di Rende, Cosenza, Italy.

[8]Instituto de Biología Molecular y Celular, Universidad Miguel Hernández, Edificio Torregaitán, Avda. del Ferrocarril s/n, 03202 Elche, Alicante, Spain.

[#]These authors contributed equally to this work

*Corresponding author addresses:
José Luis Neira, email: jlneira@umh.es Instituto de Biología Molecular y Celular, Universidad Miguel Hernández, Edificio Torregaitán, Avda. del Ferrocarril s/n, 03202 Elche, Alicante, Spain. Phone: + 34 966 65 84 59
Juan Iovanna, email: juan.iovanna@inserm.fr Centre de Recherche en Cancérologie de Marseille (CRCM), INSERM U1068, CNRS UMR 7258, Aix-Marseille Université and Institut

Paoli-Calmettes, Parc Scientifique et Technologique de Luminy, 163 Avenue de Luminy, 13288 Marseille, France. Phone 33 (0) 491 828803 Mobil Phone 0760988158 Fax 33 (0) 491 826083

Abstract

Intrinsically disordered proteins (IDPs) are emerging as attractive drug targets by virtue of their prevalence in various diseases including cancer. Drug development targeting IDPs is challenging because they have dynamical structure features and conventional drug design is not applicable. NUPR1 is an IDP playing an important role in pancreatic cancer. We previously reported that Trifluoperazine (TFP), an antipsychotic agent, was capable of binding to NUPR1 and inhibiting tumors growth. Unfortunately, TFP showed strong central nervous system side-effects. In this work, we undertook a multidisciplinary approach to optimize TFP, based on the synergy of computer modeling, chemical synthesis, and a variety of biophysical, biochemical and biological evaluations. A family of TFP-derived compounds was produced and the most active one, named **ZZW-115**, showed a dose-dependent tumor regression with no neurological effects and induced cell death mainly by necroptosis. This study opens a new perspective for drug development against IDPs, demonstrating the possibility of successful ligand-based drug design for such challenging targets.

Introduction

NUPR1 was first described as being activated in the exocrine pancreas in response to the cellular injury induced by pancreatitis (1). Subsequently, the inducible expression of *Nupr1* was discovered to be a common response to many stresses (2, 3), including minimal ones (4) in almost all cells. Moreover, NUPR1 was found to be overexpressed in some, if not all, cancer tissues compared to healthy tissue, making NUPR1 an excellent target for cancer treatment. From a molecular point of view, NUPR1 binds to DNA in a manner similar to other chromatin proteins (5, 6) for controlling the expression of gene targets (7). At the cellular level, NUPR1 participates in many cancer-associated processes including cell-cycle regulation, apoptosis (8, 9), senescence (6), cell migration and invasion (10), development of metastasis (11) and DNA repair responses (12). Indeed, NUPR1 has recently elicited significant attention due to its role in promoting cancer development and progression in the pancreas (7, 13). Notably, NUPR1-dependent effects also mediate resistance to anticancer drugs (14-16). Moreover, we have previously showed that genetic inactivation of *Nupr1* antagonizes the growth of pancreatic cancer (10, 17), and other laboratories have also shown that genetic inactivation of *Nupr1* stops the growth of hepatocarcinoma (18), non-small lung cancer (19), cholangiocarcinoma (20), glioblastoma (21), multiple myeloma (22-24), and osteosarcoma (25), thereby supporting a role for this protein as a promising therapeutic target for developing new therapies for cancers.

Structurally, NUPR1 is an intrinsically disordered protein (IDP) with an entirely disordered conformation (5, 26-29), and consequently the target-based high throughput screening for drug-selection towards this protein is highly challenging. In fact, drug-targeting IDPs is difficult due to their extremely dynamic nature, typically weak binding affinities with their natural partners, and the fact that many of them have usually several binding hotspots. Trying to use NUPR1 as a model IDP to be drug-targeted, we recently developed a combination of biophysical, biochemical, bioinformatic and biological approaches for a molecular screening in vitro, in vivo, in silico and in cellulo to select potential drug candidates against NUPR1. To this aim, we had previously followed a bottom-up approach (30). We have first characterized in vitro the interactions between NUPR1 and the potential ligands by using a collection of 1120 FDA-approved compounds. We have employed a

screening method based on fluorescence thermal denaturation (31), and identified the well-known antipsychotic agent Trifluoperazine (TFP) and its structurally related Fluphenazine hydrochloride as ligands inducing significant differences in the temperature denaturation profile for NUPR1. Phenotypic assays have been carried out to assess the potential bioactivity of TFP, as selected from biophysical screenings. Cell viability assays in the presence of TFP have led to IC_{50} of around 10 μM. Tests of TFP in vivo with human pancreatic cancer cells-derived xenografts implanted into immunocompromised mice have shown a tumor volume increase of only 50% compared to the control, whereas in mice treated with a higher dose of TFP the tumor growth has been rapidly and almost completely stopped (30). Therefore, we have previously successfully repurposed TFP as a possible cancer drug for treating pancreatic ductal adenocarcinoma (PDAC). Unfortunately, high doses of TFP also led to neurological effects on treated mice such as strong lethargy and hunched posture. Although relatively efficient as an anticancer agent, the neurological effects observed in mice preclude the use of TFP in clinics to treat cancers. For this reason, in this work we developed a multidisciplinary approach to improve the compound by, on one hand, increasing its anticancer effect and, on the other hand, reducing its undesirable neurological side-effects. In fact, a rational, in silico ligand-design guided the organic synthesis of TFP-derived compounds, which showed a stronger affinity in vitro for NUPR1, as indicated by a combination of spectroscopic and biophysical studies. One of these hit, named **ZZW-115**, showed a very evident antitumor activity via interacting with NUPR1, therefore being a promising candidate for PDAC treatment, as well as in other cancers. Furthermore, we observed that this compound induced cell death by necroptotic and apoptotic mechanisms, with a concomitant mitochondrial metabolism failure that triggers lower production of ATP and reactive oxygen species (ROS) overproduction. This work also demonstrated how the repurposing of a drug can be used as a starting point to improve the design and the efficiency of better drugs against cancer, even for challenging targets such as IDPs , and constitutes an innovative example of successful ligand-based (as opposed to structure-based) design of an inhibitor for an entirely unfolded protein.

Results

Ligand-based design and synthesis of the Trifluoperazine-derived compounds

Drug design via targeting NUPR1: The first step in the development of TFP-derived compound was to carry out in silico a ligand-based rational design, also known as "indirect" drug design. In brief, starting from the structure of TFP, we defined models of the target regions of NUPR1 that are prone to coordinate this ligand, although in a context of high molecular flexibility. To this aim, molecular dynamics (MD) simulation of NUPR1 was performed, and short fragments of the protein (up to seven amino acid residues) were used as receptors for molecular docking of TFP. These relatively small protein-ligand anchoring locations were completed with docking of additional fragments of NUPR1, and the resulting complexes were further refined by MD simulations. The complexes obtained (**Figure 1A**), which mimic highly flexible and possibly transient protein binding locations, were used as models to *i*/ identify the most important chemical moieties of TFP in the interaction with NUPR1; and *ii*/ design modifications of the drug within this template ligand. The results showed that the phenothiazine and the attached trifluoromethyl group are important for TFP to maintain coordination with the protein, with average binding energy of -7.0 kcal/mol for the parent ligand. The rest of the ligand structure is progressively less critical in anchoring to NUPR1, and may provide entropic more than enthalpic contributions to the binding. On these bases, molecular modifications were explored in the propyl linker between the phenothiazine and piperazine ring, and in the methyl group attached to the latter (**Figure 1B**). Variations in the length of the linker were found to be not significantly effective in improving the docking of TFP-derived compounds, due to a reduction in the enthalpic component of the binding. Thus, this left the methyl group as the most suitable region to modify for obtaining new active analogs of TFP for inhibiting NUPR1, and we focus our synthetic effort on changing this methyl group. Improvements in the binding energies with the methyl group substitution were up to -0.5 kcal/mol, although they depended upon the specific modification and showed a typical uncertainty of the same order of the variation estimated.

Compound synthesis: The structure of the synthesized TFP-derived compounds **ZZW-111**, **ZZW-112**, **ZZW-115** and **ZZW-116** is presented in **Figure 1C**. All the target compounds can be prepared starting from 2-(trifluoromethyl)-10H-phenothiazine, which was coupled with 1,3-dibromepropane and further various piperazine analogues to afford the TFP analogue bearing different functional groups in the piperazine moiety (**Figure 1C**). Moreover, the

hydrochlorides of these compounds (**ZZW-119**, **ZZW-120** and **ZZW-124**) were also synthesized to obtain the corresponding water-soluble candidates (**Figure 1C**).

Fluorescence, NMR, CD and ITC studies of the candidate compounds

Fluorescence: With the TFP-derived compounds predicted *in silico* in hand we then screened the selected compounds following a fluorescence-based strategy to identify the hits which could bind to NUPR1: *i*/ acquisition of the intrinsic fluorescence spectra of NUPR1 (which only contains two Tyr residues) either in the absence or presence of the TFP derivatives; and *ii*/ acquisition of the fluorescence spectra of the probe ANS (8-anilinonaphtalene-1-sulfonic acid) when NUPR1 was either isolated in solution or in the presence of the compounds. In the two strategies we were trying to monitor whether there were changes in the environment around, respectively, the two Tyr residues in NUPR1, or in the environment around where ANS binds to NUPR1 (**Figure 1D** and **Figure S1A**). By using both fluorescent approaches we were able to show that *i*/ the region around Tyr30 and Tyr36 of NUPR1 changed its conformation in the presence of any of the ZZW compounds (**Figure S1A**); and *ii*/ ANS fluorescence also varied in the presence of the TFP derivatives, indicating that ANS competes for solvent-exposed hydrophobic patches of NUPR1, with the compounds. Thus, the above results revealed that there was binding of NUPR1 to any of the compounds, and that such binding occurred around the 30s region of the sequence and altered some solvent-exposed hydrophobic patches of NUPR1.

CD: We also acquired far-UV circular dichroism (CD) experiments with some selected compounds, **ZZW-116** and **ZZW-115**; the presence of DMSO, used to prepare the stock solutions of the compounds, precluded the acquisition of many of the CD spectra (either that of the isolated compound or in the presence of NUPR1), as it absorbs strongly at short wavelengths. The aim of using CD as a spectroscopic probe is to determine whether NUPR1 modified its secondary structure in the presence of the compounds. The results with **ZZW-115** and **ZZW-116** (**Figure S1B**) indicate that none of the compounds change the secondary structure of the protein (as it is further confirmed by the NMR results, see below).

NMR: Once we had spectroscopically determined that there was binding between NUPR1 and the compounds, we aimed to verify whether the NUPR1 binding region was the same as observed for TFP (30). Thus, 2D ^{1}H- ^{15}N- HSQC NMR experiments were carried out with ^{15}N-labelled NUPR1, and for all the compounds we found there were not changes in the chemical shifts of the cross-peaks of NUPR1 (**Figure S1C**), but rather variations in their intensities upon addition of any of them (**Figure S1D**). This indicates that NUPR1 remained disordered upon binding to the compounds and no new secondary or tertiary structures were acquired. The protein residues whose cross-peak intensity was affected upon addition of the ZZW compounds are indicated in **Table 1**. When compared to the TFP, all the compounds affected the intensities of the cross-peaks of a similar set of residues, namely those around the 20s region and those at the C terminus of the protein. Besides TFP-derived compounds showing the largest number of protein residues of NUPR1 affected in the binding were **ZZW-111** and **ZZW-112**. Thus, we can conclude that there was binding between the compounds and NUPR1, and that this binding is not unspecific, since only a subset of residues were affected.

Isothermal titration calorimetry (ITC): The interaction between TFP-derived compounds and NUPR1 was further studied by ITC, the gold-standard technique in binding affinity determination, and the affinity, enthalpy and stoichiometry of binding were determined at 25°C. From the thermogram (thermal power as a function of time), the binding isotherm (ligand-normalized heats as a function of the molar ratio) was obtained through integration of the individual heat effect associated with injection of each ligand solution. Non-linear least squares regression analysis employing a model considering a single binding site in NUPR1 allowed the estimation of the binding parameters such as dissociation constant, binding enthalpy, and stoichiometry. All compounds exhibited dissociation constants in the low micromolar range (**Table 1)**. Among them, **ZZW-115** was the strongest binder, with a dissociation constant close to 2 μM (**Figure 1E**).

Effect of Trifluoperazine-derived compounds on pancreatic cancer cells growth

Treatment of MiaPaCa-2 (a traditional cell line), 02.063 and LIPC (basal subtype), Foie8b (derived from a liver metastasis) and HN14 (classical subtype) cells with compounds **ZZW-112**, **ZZW-116**, **ZZW-120** and **ZZW-124** showed an effect on cell growth which was close to

that induced by TFP, whereas treatment with **ZZW-111** and **ZZW-119** was two to three times more efficient in decreasing cell growth. Remarkably, treatment with **ZZW-115** was around ten times more efficient than with TFP (**Figure 2A** and **Table 2**). Altogether, these data strongly suggested that: *i*/ the effect of these TFP-derived compounds seemed to be independent of the subtype of pancreatic cancer cells; *ii*/ **ZZW-115** was the most efficient compound to kill the pancreatic cancer cells; *iii*/ **ZZW-111** and **ZZW-119** had an intermediate activity compared to TFP; and, *iv*/ **ZZW-112**, **ZZW-116**, **ZZW-120** and **ZZW-124** had an antiproliferation activity similar to TFP. Moreover, **ZZW-115** antitumor activity was tested on a panel of 11 primary PDAC-derived cells and it was found to be efficient to kill the cancer cells with IC_{50} in the range from 0.84 µM (ANOR) to 4.93 µM (HN14), a very small therapeutic window (**Figure 2B)**. These in vitro results are therefore in good agreement with the findings of ITC measurements, in which **ZZW-115** is the compound inducing the greatest affinity and therefore resulted in best anticancer activity. Moreover RNA-seq data showed that NUPR1 expression is systematically overexpressed in PDAC cells, but small differences between cell lines were founded. Finally, NUPR1 expression was plotted against the AUC (area under the curve) after **ZZW-115**-treatment and no significant correlation was found (**Figure 2C)**. In this regard, we cannot cluster cell lines in low/high expression or low/high sensibility.

Since resistance to chemotherapy is a common issue that oncologists must face in the treatment of patients with PDAC, we used the MiaPaCa-2 cell line, which has become resistant to the two chemotherapeutic agents oxaliplatin or gemcitabine, to assess whether resistance to them is also conferring resistance to **ZZW-115**. Remarkably, **ZZW-115**-treatment of resistant MiaPaCa-2 cells showed the same sensitivity as the parental cells, as demonstrated in **Figure 2D**. We hence suggest that the antitumor effect of the **ZZW-115** is not influenced by the resistance to others drugs and may affect some other intracellular pathways.

Finally, to verify that **ZZW-115** displays its anticancer activity via targeting NUPR1, we incubated Panc1 cells wild-type (NUPR1 WT) or with inactivated *NUPR1* (NUPR1 KO) in the presence of **ZZW-115**. As shown in **Figure 2E**, NUPR1 KO cells are significantly more resistant to **ZZW-115**-treatment at different time points after challenging them with increasing concentrations of the compound. For example, after 72 h of treatment with 15 µM of **ZZW-**

115, only 15.01 ± 4.58% of NUPR1 WT cell survived compared to 84.60 ± 3.84% of NUPR1 KO cells. These results indicated that probably **ZZW-115** was exerting its effect by binding to NUPR1. Although it is not unambiguously proved that NUPR1 is the only protein that **ZZW-115** could target, our results showed that targeting NUPR1 may be the main mode of action of **ZZW-115**, and the ligand-protein binding contributed to its antitumor effect.

Altogether, these above data showed that **ZZW-115** was capable of efficiently killing the pancreatic tumor cells lines *via* targeting NUPR1, with no distinction regarding the PDAC subtype, or even if the cells are resistant to the classical drugs currently used in the clinical practice.

ZZW-115 inhibits the growth of other tumors-derived cells

Since NUPR1 is overexpressed in several (if not all) tumors, we evaluated the effect of the treatment in cellular lines derived from other different tumors concentrations of **ZZW-115**. Treatment of cells such as U87 (glioblastoma), A375 and B16 (melanoma), U2OS and SaOS-2 (osteosarcoma), HT29, SK-CO-1 and LS174T (colon cancer), H1299 and H358 (lung cancer), HepG2 (hepatocarcinoma), PC-3 (prostate), THP-1 (acute monocytic leukemia), Daudi (lymphoma), Jurkat (acute T cells leukemia) and MDA-MB-231 (breast cancer), demonstrated that **ZZW-115** was efficient to kill these tumor cells with IC_{50} in the range from 0.42 µM (Hep2G cells) to 7.75 µM (SaOS-2 cells) (**Figure 2F)**. These data displayed that **ZZW-115** could be potentially active for treating cancers from various tissues by targeting NUPR1.

ZZW-115 inhibits the growth pancreatic xenografted tumors in vivo

Because the compound **ZZW-115** was the most efficient candidate for treating cancer cells in vitro, we therefore selected it to treat MiaPaCa-2 cells-xenografted mice. We applied a protocol similar to that previously used for validating TFP in vivo (30). When tumors reached 200 mm^3 we started a daily treatment, for 30 days, with 5, 2.5, 1.0 or 0.5 mg/kg of **ZZW-115**, whereas the control group received an equivalent volume of vehicle solution. As expected, tumor volumes increased in an exponential manner in control mice (from 217.7 ± 16.7 mm^3 to 1790.7 ± 97.0 mm^3 during the 30 days of observation). In contrast, when the mice were injected with **ZZW-115** at 5 mg/kg, the tumors stopped growing a few days after treatment

and, furthermore, their size decreased progressively up to almost disappear at the end of the treatment (from 205.9 ± 23.7 mm^3 to 134.2 ± 106.8 mm^3; 27.4 ± 4.6 mm^3 when excluding the outlier mouse). In the outlier mouse the tumor showed a decrease in the growth, but it did not disappear completely (**Figures 3A, 3B** and **3C)**. Moreover, mice treated with 2.5 mg/kg showed a tumor growth from 191.9 ± 23.7 mm^3 to 779.6 ± 189.8 mm^3 at 30 days (603.9 ± 27.6 mm^3 when excluding one outlier mouse), tumors from mice treated with 1.0 mg/kg grew from 269.5 ± 27.6 mm^3 to 1045.4 ± 266.1 mm^3, and those treated with 0.5 mg/kg from 238.6 ± 29.6 mm^3 to 1574.6 ± 237.4 mm^3. These data clearly show a dose-dependent effect with almost no significant outcome in animals treated with the lowest doses. Notably, contrary to what we observed for the TFP treatment (30), we did not find any appreciable neurological side-effects, including in a 30-day period of treatment with 10 mg/kg (data not shown). Moreover, in an independent 5 mg/kg-treated group, we stopped the treatment after 30 days and followed the tumor growth for additional 30 days. The results presented in **Figure 3D** show that the growth arrest on the tumors was dependent on the **ZZW-115** administration, since the remaining tumor started growing again after suspension of the drug administration. Three additional primary PDAC-derived cells (LIPC, AOIPC and HN14) were xenografted and treated for 30 days with 5 mg/kg of **ZZW-115** and observed that tumor volume decreased (**Figure 3E**). Moreover, immunocompetent C57BL/6 mice were orthotopically implanted with Panc02 cells, treated with 5 mg/kg of **ZZW-115** for 30 days and observed that tumor size resulted almost unmeasurable in some cases (**Figure 3C**). In addition, histological analysis of the tumors, after the 30 days of treatment with **ZZW-115**, showed obvious areas of necrosis as shown in **Figure 3F**. Furthermore, numerous apoptotic cells were also observed.

We then evaluated the effect of **ZZW-115** on the PDX1-Cre; $Kras^{G12D}$; $Ink4a^{flox/flox}$ mice model. This animal model can spontaneously develop an aggressive PDAC that leads to the mice death at the age of 9 to 10 weeks. We started the daily **ZZW-115**-treatment (5 mg/kg) at week 5 of life and then sacrificed the mice at the end of week 8. Importantly, the pro-necrotic effect induced by **ZZW-115** was still noticeable after 3 weeks of treatment in PDX1-Cre;$Kras^{G12D}$;$Ink4a^{flox/flox}$ mice (**Figure 3F)**. The percentage of necrotic area in the tumors was calculated by histological analysis after hematoxilin and eosin (H&E) staining. We found a significant increase of necrosis in **ZZW-115**-treated mice, from 10% to 43% of the surface

area in some tumors, whereas in the PDAC from the untreated mice these areas were in the ranged from 0 to 3.5% (**Figure 3G)**. We hence conclude that **ZZW-115** could disrupt tumor growth (at low doses) and could reduce tumor size (at high doses) for the xenografted tumors, without obvious neurological side-effects in the mice.

ZZW-115 induces pancreatic cell death by necrosis and apoptosis

Although **ZZW-115** treatment kills cancer cells and decreases the size of the xenografted pancreatic cancer tumors, details of its molecular mechanism are unknown. Prompted by our results described above, we measured the necrotic and the apoptotic effects throughout the LDH release and caspase 3/7 activity, respectively, in several pancreatic primary cancer cells. Upon **ZZW-115** treatment, we found that LDH release was significantly higher in **ZZW-115-**treated cells than in control ones in a concentration-dependent manner as presented in **Figure 4A** and **Figure S2A**. Similarly, caspase 3/7 activity was also larger in **ZZW-115**-treated cells, as showed in **Figure 4B and Figure S2B**. Taken together, these experiments demonstrated that **ZZW-115** exerted both pro-necrotic and pro-apoptotic effects. We also used flow cytometry after co-labelling cells with Annexin V and PI to measure apoptosis and necrosis, respectively, in **ZZW-115**-treated cells. Treatment with **ZZW-115** increased necrotic and apoptotic events, as presented in **Figure 4C and Figure S3A**, which agrees with the data concerning LDH release and caspase 3/7 activity, respectively. Moreover, analysis of nuclear shape of PI-stained cells corroborates the combination of pro-apoptotic and pro-necrotic effects of **ZZW-115** treatment (**Figure S3B**). Altogether, these findings indicate that **ZZW-115**-treatment induced cell death by both mechanisms: necrosis and apoptosis. Interestingly, pretreatment of MiaPaCa-2 cells with the pan-caspase inhibitor Z-VAD-FMK and/or the necrosis inhibitor Nec-1, prevented LDH release (**Figures 4D)**. For example, in a 5 µM **ZZW-115** treatment, preceded by Z-VAD-FMK pretreatment, reduced the LDH to 70%, Nec-1 pretreatment reduced it to 52%, and the combination of both inhibitors to 46%. At the same concentration of **ZZW-115**, pretreatment with Z-VAD-FMK inhibited drastically the caspase 3/7 activity, whereas Nec-1 treatment did not affect this activity (**Figure 4E)**. In line with these results, we performed rescue experiments on a panel of PDAC primary cells by incubating them with increasing concentrations of **ZZW-115** in combination with either Z-VAD-FMK, Nec-1, or both. Our results show that both inhibitors can improve cell viability,

the treatment with Nec-1 being more efficient, indicating that **ZZW-115** induces necroptosis and apoptosis by independent mechanisms (**Figure 4F**).

Moreover, we compared the **ZZW-115** to the paclitaxel, a standard pro-apoptotic drug, used in PDAC treatment, in order to elucidate whether their effects overlapped. To this end, we measured LDH release and caspase 3/7 activity at different times. Both drugs used alone induced a similar caspase activity and, as expected, Z-VAD-FMK prevented almost completely such activation, showing that both compounds stimulated a caspase-dependent apoptosis to a similar extent in PDAC cells (**Figure 4G**). Interestingly, LDH release was five times lower in paclitaxel-treated cells compared to **ZZW-115**-treatment, and incubation with Z-VAD-FMK, had significant effect, reducing LDH release on both paclitaxel and **ZZW-115** treatments (Figure 4H). Remarkably, pretreatment with Nec-1 did not reduced the caspase activation in both **ZZW-115** and paclitaxel treatments (**Figure 4I**). However, and most importantly, incubation with Nec-1 only induced a significant rescue in **ZZW-115**-treated cells but not in paclitaxel-treated cells (**Figure 4J**). Our data support the idea that **ZZW-115-** treatment strongly induces programmed cell death by both necrosis and apoptosis with small, if any, interdependency between the two pathways.

ZZW-115 treatment induces metabolic failure

ATP production is essential for most cellular processes, and its monitoring is a good marker to understand the metabolic changes undergoing during cell death. In this regard, we evaluated the ATP content in **ZZW-115**-treated cells. Remarkably, we found that the levels of ATP were significantly reduced in cells treated with **ZZW-115** in a concentration-dependent manner on a panel of PDAC-derived primary cells (**Figure 5A**), as well as on other cancerous ones (**Figure S4A**). Consequently, we deeply investigated whether this decrease in the intracellular ATP content might be the result of reduced efficiency of the mitochondrial metabolism or anaerobic glycolysis. Therefore, we evaluated different mitochondrial parameters such as basal respiration, maximal respiration, spare capacity and ATP production by mitochondrial respiration, reflected in the oxygen consumption rate (OCR). Hence, we measured the OCR in MiaPaCa-2 cells after 4, 8 and 24 hours in the presence of **ZZW-115** (**Figure 5B**). Interestingly, compared with untreated cells, we observed a time-

dependent variation in the mitochondrial respiration, with a significant decrease of all the mitochondrial parameters after 8 hours of incubation with **ZZW-115**. Interestingly, the mitochondrial respiration failure induced by **ZZW-115** treatment is not specific to the PDAC cells, as it was also found for other cancer cell lines (**Figure S4B**). Since O_2-dependent ATP production was also affected in **ZZW-115**-treated cells, we evaluated the energy production by anaerobic glycolysis, measuring the extracellular acidification rate (ECAR) by the proton efflux into the media during lactate release. These experiments demonstrated that the cells shifted to anaerobic glycolytic metabolism between 4 and 8 hours after **ZZW-115** treatment (**Figure 5C**), similar to the shift observed following a mitochondrial failure (32). Besides, this switch is transitory because cells metabolize rapidly their glycolytic reserve on a time dependent manner losing, also, their glycolytic capacity. Again, this glycolytic capacity failure after **ZZW-115**-treatment was also confirmed in various pancreatic primary cancer cells, as well as in other cancer cell lines (**Figure S4C**). By calculating the total ATP production by the two different pathways, we observed a significant time-dependent decrease of ATP production from mitochondrial metabolism, as well as transient increase of glycolytic ATP-production with a significant decrease of total ATP production after 8 hours of treatment (**Figure 5D**).

As it is well-known, mitochondrial dynamics is related to the cell death pathways. Mitochondrial dysfunction, including decreased respiration and oxidative phosphorylation (OXPHOS), metabolic shift towards glycolysis, and increased mitochondrial ROS-formation, leads to the activation of pro-survival or pro-death pathways depending on the stimulus (33). In this regard, we were interested in understanding whether mitochondrial ROS production was involved in cell death induced by **ZZW-115**. To answer this question we measured superoxide formation by using MitoSOX labelling and found a significant increase in the ROS formation (**Figure 5E)**. Moreover, in the PDAC cell lines panel, ROS production is positively correlated with the cell sensibility, and inversely correlated with the ATP production. Furthermore, to better understand the relation between the cell death and metabolism failure, we performed experiments in **ZZW-115**-treated MiaPaCa-2 cells, where we measured the ATP content after pretreatment with Z-VAD-FMK or/and Nec-1. Our results, presented in **Figure 5F**, showed that the ATP content could be restored by inhibiting both necrosis and apoptosis. Accordingly, Nec-1, which showed the most efficient rescue

capacity after **ZZW-115**-treatment, presented also a stronger ability to restore the ATP content. Moreover, Nec-1 pretreatment of **ZZW-115**-treated cells was able to increase anaerobic glycolysis whereas no improvement was found in the mitochondrial metabolism **(Figure S5)**. In this regard our results shown that Nec-1 is not able to rescue mitochondrial metabolic activity, meaning that the mitochondrial disruption takes place before the activation of the necroptosis. Consequently, RIP1 activation may not be upstream of mitochondrial dysfunction after **ZZW-115**-treatment. These data have been validated with siRNAs. Finally, we also compared treatment with paclitaxel to the one with **ZZW-115**, to elucidate whether their effects on ATP content were similar. As expected, both isolated drugs induced a time-dependent decrease in the ATP content (**Figure 5G** and **Figure 5H**), the effect being greater with **ZZW-115** and starting after 4 hours of treatment. More interestingly, both cell death inhibitors were capable of restoring the ATP content in **ZZW-115**-treated cells, whereas only the Z-VAD-FMK inhibitor was capable of increasing ATP content in paclitaxel-treated cells.

Taken together, these results strongly support a model whereby, under **ZZW-115** treatment, the induced cell death is the consequence of a decrease of ATP production by the mitochondria, accompanied with an increase of mitochondrial ROS production with a transient metabolic shift towards anaerobic glycolysis. Moreover, in agreement with our previous data, inhibition of apoptosis, and mainly necrosis by Nec-1 incubation, can restore metabolic functions and ATP content (34).

Discussion

A TFP-derived compound decreases pancreatic tumor size by acting on NUPR1.

In this work we described the synthesis and characterization of a novel TFP-derived compound with a strong anticancer effect both in vitro and in vivo, due to its capability of inducing programmed necrosis and apoptosis. Based on a modeled structure of NUPR1 and of the selected fragments of its sequence involved in ligand binding, a collection of compounds was designed and synthesized with the aim of improving the affinity towards the protein target compared to the cognate drug. The biophysical and biochemical analysis of these compounds showed that **ZZW-115** was bound to NUPR1 more favorably than TFP

(Table 1) and, in return, this compound exhibited a better anticancer effect in vitro on several primary PDAC cells, as well as on other cancer cell lines. Most importantly, **ZZW-115** was a very efficient anticancer drug candidate in vivo on mice because it was capable not only of stopping tumor growth, but also of decreasing the tumor size until its disappearance mainly due to necrosis.

TFP is an effective antipsychotic drug for people with schizophrenia (35), acting by blocking central dopamine receptors. TFP, and some of its derived compounds, were referred to have anticancer effects in some (36-39), but not in all cancer models (40), in an early attempt to repurpose the drug. However, TFP cannot be used in clinic for treating patients with cancers due to its numerous, undesirable side-effects, at efficient anticancer doses. This is why it is important to use a rational approach to develop new TFP-derived compounds, with little side-effects and higher anticancer activity. On the basis of our previous observation that TFP binds to NUPR1 and blocks its activity (30) leading to anticancer effect in PDAC, we built models of the NUPR1-TFP complex which could give us hints on how to improve the interaction with some novel derivatives. This constitutes an original ligand-based approach to the rational design of drugs against a totally unstructured protein, whereas previous pioneer attempts only included structure-based design against partly-folded IDPs (41). The capacity of interaction with NUPR1 of such new compounds was biophysically and biochemically validated by using several spectroscopic and biophysical strategies; a stronger interaction with NUPR1 was found in particular for the compound **ZZW-115** (**Table 1**), which also resulted in an improved anticancer activity both in vitro and in vivo. Noteworthy, and in contrast with TFP treatment, no apparent neurological effect was observed on mice, even at 10 mg/kg dose administrated daily for 30 days.

Inhibition of the NUPR1 activity as an anticancer strategy was evaluated and proven in pancreatic cancer (10, 17), but also in several other solid and liquid tumors such as hepatocarcinoma (18), non-small lung cancer (19), cholangiocarcinoma (20), glioblastoma (21), multiple myeloma (22-24), and osteosarcome (25). These findings indicate that **ZZW-115** could be used for treating tumors from different origins with a range of IC_{50} from 0.42 µM to 7.75 µM (**Figure 2E)**. Thus, we believe that **ZZW-115** is a promising agent for treating

various cancers due to its effectiveness in targeting NUPR1, since the protein is commonly overexpressed in many cancerous tissues.

The compound ZZW-115 acts at cellular level by promoting programmed necrosis: insights into its cellular functions.

Histological study from both PDAC mice models, xenografts and tumors from PDX1-Cre;$Kras^{G12D}$;$Ink4a^{flox/flox}$ mice, demonstrate a strong pro-necrotic effect of **ZZW-115** treatment; this effect makes **ZZW-115** an extremely original drug candidate. In this regard, we noted that only a very small number of compounds rely on the capability of inducing necrosis as the main cause of their anticancer activity. For each novel candidate proposed to become an anticancer drug, such as **ZZW-115**, an essential prerequisite is to understand its mechanism of action. Moreover, understanding the cell death pathways elicited through a potential anticancer drug represents a milestone in preclinical studies. This is why we performed several functional studies to clarify this aspect, and found that treatment with **ZZW-115** of a whole panel of pancreatic cancer cells, as well as other cancer cells, induced in all cases a programmed cell death mainly by necrosis, but concomitantly also by apoptosis. In fact, cell rescue was possible by using two distinct cell death inhibitors, i.e. Nec-1 for necroptosis and Z-VAD-FMK for apoptosis. Moreover, the combination of **ZZW-115**-induced necrosis and apoptosis offered an improvement in the treatment of cancers compared to exclusively pro-apoptotic drugs, because the former enhances their effect by providing two different mechanisms of cell death induction. Likewise, we have demonstrated that **ZZW-115** can efficiently target cells that are already resistant to pro-apoptotic drugs commonly used in clinic. In this regard, a combination of the promotion of both apoptosis and necroptosis could improve treatment against cancer cells that very frequently develop drug resistance (42).

An important question that needs to be answered is why the cancer cells are sensitive to this strong pro-necrotic compound, whereas normal cells, as observed in mice treated with high doses, up to 10 mg/kg/day during 30 days, do not show evidences of off-target effects. We suggest that this is due to the fact that cancer cells are more reliant on NUPR1-dependent pathways. In fact, we hypothesize that since cancer cells are growing under hypoxia, low

contribution of nutrients, mechanic stress and various other constrained conditions, these stress situations activate NUPR1 expression, and therefore NUPR1-dependent mechanisms can help cells to adapt to such environmental conditions. Thus, cancer cells become highly dependent on the NUPR1 activity to live and grow under stress conditions. That is, cancer cells, but not healthy ones, are probably fully dependent on a NUPR1-adaptative mechanism.

It is also interesting to note that after **ZZW-115** treatment we found a very remarkable metabolic failure due to a mitochondrial metabolism rupture. This mitochondrial failure was accompanied with an increase of mitochondrial ROS production that raised cell instability and oxidative stress. Following mitochondrial respiration stress, cells shift towards anaerobic glycolytic metabolism to compensate for the lack of ATP (32). This anaerobic shift was observed between 4 and 8 hours after the treatment with **ZZW-115** (**Figure 5C)**. Glycolysis is a less favorable ATP-producer pathway and cells rapidly consume glycolytic reserves, leading to ATP decrease, and then, to programmed cell death by both necroptosis and apoptosis. These results are in agreement with the fact that treating pancreatic cells with a siRNA against NUPR1 (34) or with TFP (unpublished data) induces a similar metabolic disruption.

Material and Methods

Computational modeling of a TFP-derived compound

MD simulations of NUPR1 were carried out in the isobaric-isothermal ensemble using the GROMACS simulation package (43) in combination with the force fields AMBER ff99SB-ILDN (44). The protein was equilibrated in explicit TIP4P-D water (45) starting from an extended conformation, following a protocol previously described (27). Fragments of the simulated protein structure with a length of 5 or 7 amino acid residues were used as receptors for molecular docking of either TFP or TFP-derived compounds, by using the AutoDock Vina software (46). The choice of using short fragments of NUPR1 was motivated not only by the necessity of reducing its exceedingly large conformational space, but also by the fact that ligand binding to the protein is dictated by local hydrophobicity spanning up to seven amino acid residues (28, 30). Furthermore, we have previously proved that molecular docking is sufficiently accurate to reveal the binding locations of drugs to NUPR1 in a blind search (30).

After docking of the ligand, the complex was considered as is or completed with addition of a second fragment of NUPR1, selected among those that had shown the most favorable affinity for the same ligand in the previous docking calculations. The resulting complexes were equilibrated by 1 ns of MD performed using the GAFF force field (47) for the compounds. Simulation conditions including treatment of the electrostatics and van der Waals interactions, and reference values and coupling times for both the thermostat and barostat, were as formerly reported (27, 29). After the MD runs, the binding affinity of the compounds was evaluated using the scoring function of AutoDock Vina (46), by performing a re-docking of the ligand in the position occupied within the average structure of the simulated complex.

Synthesis of TFP-derived compounds

The 2-(trifluoromethyl)-10H-phenothiazine (1, 204 mg), 1,3-dibromepropane (0.4 mL) and Cs_2CO_3 (150 mg) were dissolved in 1.6 mL of dimethylformamide (DMF) and stirred at 65°C for 12 h. After completion of the reaction, the solvent was removed. The residue was dissolved in ethyl acetate and washed with brine. The combined organic layer was dried over Na_2SO_4, filtered and concentrated under reduced pressure to yield crude product which was further purified by column chromatography to afford the intermediate compound 2 (96 mg, 31.8%). Then, compound 2 and piperazine (or other piperazine analogues) were dissolved in DMF and stirred at 25°C overnight. After completion of the reaction, the solvent was removed and the residue was purified by column chromatography to afford the TFP-derived compounds. The yields of **ZZW-111**, **ZZW-112**, **ZZW-115** and **ZZW-116** were 68%, 77%, 64% and 76%, respectively. The TFP-derived compounds were completely dissolved in CH_2Cl_2 at 25°C. The anhydrous HCl was bubbled through the solution for 5 minutes. Then the solvent was removed and the residue was purified by column chromatography to afford the hydrochloride salt of the TFP-derived compound with a yield of 99%.

Protein expression and purification

NUPR1 was produced and purified from transformed *E. coli* grown in LB media as previously described (5). For the production of ^{15}N- labelled samples, the cells were grown in M9

minimal media, with 1 g of $^{15}NH_4Cl$ per liter of media, supplemented with vitamins, and purified as the protein obtained from *E. coli* grown in LB media.

Fluorescence spectroscopy

Fluorescence spectra were collected in a Cary Eclipse spectrofluorometer (Varian-Agilent Technologies, Santa Clara, CA) interfaced with a Peltier-thermostated multicell holder. The slit widths were 5 nm for both excitation and emission wavelengths. Excitation wavelength was 280 nm. Emission spectra from 300 to 400 nm were acquired at 25°C, in a 1-cm-pathlength quartz cell (Hellma Analytics, Müllheim, Germany). The NUPR1 concentration was 8 μM in buffer in 20 mM sodium phosphate pH 7.0, and 50 μM of each TFP-derived were added in each experiment. For the experiments in the presence of ANS, the final concentration of the probe was 200 μM, with the same concentrations for the compound and NUPR1 as in the intrinsic fluorescence experiments. Excitation wavelength was 370 nm and emission spectra were collected from 400 to 600 nm. Slit widths were the same as before.

NMR spectroscopy

The NMR data were acquired at 25°C, pH 4.5 (acetate buffer), on a Bruker Avance DRX-500 spectrometer equipped with a triple-resonance probe and z-gradients. All spectra were referenced to external TSP (48). The 2D ^{1}H-^{15}N heteronuclear single-quantum coherence (HSQC) spectra were acquired either for isolated ^{15}N-labelled NUPR1 (100 μM), or alternatively for ^{15}N-labelled NUPR1 (100 μM) in the presence of the corresponding TFP-derived compound (400 μM). Frequency discrimination in the indirect dimensions was achieved by using the echo/antiecho-TPPI method (48). The spectra were acquired with 1 K complex points in the ^{1}H dimension, 128 complex points in the ^{15}N dimension, and 200 scans. The carrier of the ^{1}H dimension was set at 8.00 ppm, and that of ^{15}N at 120 ppm. The spectral widths used were 10 and 35 ppm in the ^{1}H and ^{15}N dimensions, respectively. Water signal was suppressed with the WATERGATE sequence (49). Data were zero-filled to double the number of original points in both dimensions, apodized with shifted squared sine-bell functions in the two dimensions and Fourier transformed with the program TopSpin 2.1. Assignments were taken from those previously reported for NUPR1 (26). The intensity of the

signals from each row in the HSQC spectra was measured by using TopSpin 2.1 and taking into account, as an internal reference, the intensity of the last residue of NUPR1. Only differences in intensity of a particular protein residue between spectra of the complex (NUPR1:compound) and that of isolated NUPR1 were considered significant only larger than 10%.

Far-UV circular dichroism spectroscopy

The far-UV CD experiments were acquired in a Jasco J815 spectropolarimeter (Jasco, Japan) with a thermostated cell holder, and interfaced with a Peltier unit, at 25 °C. The instrument was periodically calibrated with (+)-10-camphorsulphonic acid. A path length cell of 0.1 cm was used (Hellma). Spectra of the isolated molecules (NUPR1 or the corresponding compound) were acquired at a scan speed of 50 nm/min with a response time of 2 s and averaged over 6 scans with a bandwidth of 1 nm. Concentration was 20 μM of each molecule either in isolation or when forming the complex. The buffer used was phosphate buffer at pH 7.0 (50 mM).

Isothermal titration calorimetry (ITC) assays

The binding of the TFP-derived ZZW compounds to NUPR1 was determined with a high sensitivity isothermal titration calorimeter Auto-iTC200 (MicroCal-Malvern Panalytical). Protein samples and solutions were properly degassed. Experiments were performed with freshly prepared protein solutions at 25°C. A solution of NUPR1 (20 μM, in sodium phosphate 20 mM, pH 7.0, 2% DMSO) in the calorimetric cell was titrated with a solution of each compound (200 μM, in sodium phosphate 20 mM pH 7.0, 2% DMSO). A standard protocol was employed: 19 titrant injections with 2 μL of compound solution were programmed with a time spacing of 150 s, a stirring speed of 750 rpm, and a reference power of 10 μcal/s. The heat evolved after each ligand injection was obtained from the integral of the calorimetric signal. The heat due to the binding reaction was obtained as the difference between the reaction heat and the corresponding heat of injection, the latter estimated as a constant value throughout the experiment, and included as an adjustable parameter in the analysis. Control experiments (with ZZW compounds injected into buffer) were performed under the same experimental conditions. The association constant (K_a) and

the enthalpy change (Δ*H*) of the binding reaction were obtained through non-linear regression analysis of experimental data to a model assuming a single ligand binding site for the protein. Experiments were performed in replicates and data were analyzed using in-house developed software implemented in Origin 7 (OriginLab, Northampton, MA).

Cell viability assays

Cell viability after treatment was assessed in cancer cell lines: MiaPaCa-2 and Panc-1 (pancreatic cancer), U87 (glioblastoma), A375 and B16 (melanoma), U2OS and SaOS (osteosarcoma), HT29, SK-CO-1 and LS174T (colon cancer), H1299 and H358 (lung cancer), HepG2 (hepatocarcinoma), PC3 (prostate), Jurkat (acute T cells leukemia) and MDA-MB-231 (breast cancer). Cells were obtained from ATCC (Manassas, VA) and maintained in Dulbecco's Modified Eagle's Medium (DMEM) (Invitrogen, Carlsbad, CA) supplemented with 10% Fetal Bovine Serum at 37 °C with 5% CO_2. The primary pancreatic cancer-derived cells were cultured as previously described (50). Cells were plated in 96-well plates (5.000 cells/well). Twenty-four hours later, the media were supplemented with 0 to 100 µM concentration of the compound to be tested, and were incubated for another additional 24 or 72 hours. Cell viability was estimated after addition of the CellTiter-Blue viability reagent (Promega, Madrid, Spain) for 3 h according to the protocol provided by the supplier. Cell viability was normalized with respect to untreated cells rates.

Animals

Female NMRI-Foxn1^{nu}/Foxn1^{nu} mice (nude mice) were provided by Janvier Laboratories (Le Genest-Saint-Isle, France). Male C57BL/6 mice were obtained from Charles River Inc. Male Pdx1-Cre;Ink4a/Arf$^{fl/fl}$;LSL-Kras^{G12D} mice were obtained by crossing the following strains: Pdx1-Cre;Ink4a/Arf$^{fl/fl}$ and LSL-Kras^{G12D}. Mice were kept within the Experimental Animal House of the Centre de Cancérologie de Marseille, pôle Luminy. Ten millions MiaPaCa-2 cells were inoculated subcutaneously in nude mice (8 weeks old) and they were separated into 5 groups of 6 subjects each. Ten millions LIPC, AOIPC and HN14 cells were subcutaneously injected in nude mice and separated in 2 groups (treated and untreated). In C57BL/6 mice (9 weeks old), Panc02 cells (3×10^5) were injected with a 30G needle in the tail of the pancreas and the peritoneum and skin were closed with 5-0 prolene sutures. Mice were treated daily

with 0.5% DMSO in physiologic serum (vehicle), 5, 2.5 , 1.0 or 0.5 mg/kg of **ZZW-115** when the tumor volume reached 200 mm^3. Every 5 days, the mice weight and the tumors volumes were measured. Mice were sacrificed after 30 days of treatment. In an independent group of 6 mice, animals were xenografted and treated with 5 mg/kg of **ZZW-115** during 30 days as described above but the tumor growth was followed by an additional 30 days-period without any additional treatment.

Necrosis evaluation

To perform necrosis evaluation of the tumor, formalin-fixed samples were embedded in paraffin and 5-µm sections were stained with hematoxilin and eosin (H&E). Percentage of necrotic area was calculated by the ImageJ program.

CRISPR-Cas9 clones development

Cells were seeded and transfected with 1 µg of *NUPR1* double nickase plasmid or double control nickase plasmid (Santa Cruz Biotechnology, Heidelberg Germany), using Lipofectamine 3000 Transfection Reagent (Thermo Fisher Scientific, Carlsbad, CA) in each well, following the manufacturer's protocol. Transfected cell selection was performed with puromycin and, after 72 h, single cell colonies were isolated. Complete allelic knockouts were confirmed using Sanger sequencing.

siRNA transfection

Cells were plated at 70% confluence and INTERFERin reagent (Polyplus-transfection) was used to perform siRNA transfections, according to the manufacturer's protocol. Scrambled siRNA that targets no known gene sequence was used as a negative control. Assays were carried out 72 h post-transfection.

LDH assay, ATP production, and caspase-3/7 activity assay

MiaPaCa-2 cells were seeded at a density of 10,000 cells/well in 96-well plates. Cells were allowed to attach overnight and treated the next day for 24 h with different concentrations of **ZZW-115**. At the end of the experiment, LDH release, ATP production, and caspase-3/7 activity were monitored using CytoTox-ONE (Promega G7890, Madison, WI), CellTiter-Glo

(Promega G7571, Madison, WI) and Caspase-Glo 3/7assay (Promega G8091, Madison, WI), respectively. Data were normalized with respect to the cell number.

OXPHOS and glycolitic metabolism measurements

Measurements were performed using a Seahorse Bioscience XF24 Extracellular Flux Analyzer. Cells were plated at 30,000 cells/well onto Seahorse 24-well plates 48 h before the assay, and treated 24 h later with **ZZW-115**. The OCR (pmoles/min) was measured using the XF Cell Mito Stress Test Kit (Agilent, Wilmington, DE) under basal conditions, and in response to 1 µM oligomycin, 0.25 of carbonylcyanide p-(trifluoro-methoxy)phenylhydrazone (FCCP) and rotenone and antimycin A (0.5 µM each), (Sigma, Saint Louis, MO). ECAR (mpH/min) was measured using the Seahorse XF Glycolysis Stress Test Kit (Agilent, Wilmington, DE) at basal conditions and upon glucose (10 mM), oligomycin (1 µM) and 2-Deoxyglucose (100 mM) addition (Sigma, Saint Louis, MO). The contribution of OXPHOS and glycolysis to ATP production was calculated using the OCR and PPR as previously described (51).

AnnexinV/PI staining

Cells were collected after incubation for 24 h of treatment with **ZZW-115**. Cells were washed and then detached with Accutase (Gibco, Life Technologies, Carlsbad, CA), and resuspended in Annexin-binding buffer. Pacific-Blue Annexin V (5 µL, BioLegend, San Diego, CA) was added to the cell suspension and incubated during 15 min. Before analysis by flow cytometry, propidium iodide (5 µL, Miltenyi Biotec, Surrey, UK) was added to the suspension. 10,000 events per sample were collected in a MACSQuant-VYB (Miltenyi Biotec). Data analysis was performed using the FlowJo software.

Superoxide anion production by the mitochondria

MitoSOX (Molecular Probes, Eugene, OR) was added to a final concentration of 5 µM for 10 min. After incubation, cells were washed with warm PBS, detached with Accutase, and resuspended in HBSS (Gibco, Life Technologies, Carlsbad, CA) for flow cytometry. 10,000 events per sample were collected in a MACSQuant-VYB, and data analysis was performed using FlowJo software.

Statistics

Statistical analyses were performed by using the unpaired 2-tailed Student t-test; either non-normal distribution, 1-way ANOVA or 2-way ANOVA with Bonferroni post-hoc test were also used when appropriate. IC_{50} and the area under the curve (AUC) values were calculated by non-linear regression curves with robust fit using GraphPad software. Values are expressed as mean ± SEM. Data are representative of at least three independent experiments with technical triplicates completed. P value less than 0.05 was considered significant.

Study approval

All experimental protocols were carried out in accordance with the nationally approved guidelines for the treatment of laboratory animals. All experimental procedures on animals were approved by the Comité d'éthique de Marseille numéro 14 (C2EA -14).

Author contributions

PSC, WL, ZZ, CH, PS, AVC, OA, BR and JLN conducted experiments. PSC, YX, LP, BR, JLN and JI contributed to study design and reviewed and revised the manuscript. PSC, JLN and JI analyzed and interpreted the data. PSC, YX, PS, BR, JLN and JI wrote the manuscript. JI designed and supervised the study.

Conflict of interest

PSC, YX, LP, AVC, OA, BR, JLN and JI have a pending patent entitled "NUPR1 Inhibition for treating cancer" filed on May 31st 2018 (European Patent Application n.EP18305672.0).

Acknowledgments

This work was supported by La Ligue Contre le Cancer, INCa, Canceropole PACA and INSERM to JI; Miguel Servet Program from Instituto de Salud Carlos III (CPII13/00017 to OA); Fondo de Investigaciones Sanitarias (PI15/00663 and PI18/00343 to OA; Spanish Ministry of Economy and Competitiveness (BFU2016-78232-P to AVC, CTQ2015-64445-R to JLN); Diputación General de Aragón (Protein Targets Group B89 to AVC, and Digestive Pathology Group B01 to OA); Generalitat Valenciana (Prometeo 018/2013 to JLN); and Centro de Investigación Biomédica en Red en Enfermedades Hepáticas y Digestivas (CIBERehd); Fundación Alfonso Martín-Escudero and Fondation de France to PSC; China Scholarship Council to W.L. and C.H.; Programme XU GUANGQI to YX and JI; and National Natural Science Foundation of China (81502920), the Fundamental Research Funds for the Central Universities (106112017CDJQJ468823) to YX. BR acknowledges kind hospitality in the European Magnetic Resonance Center (CERM), Sesto Fiorentino (Florence), Italy.

Bibliography

1. Mallo, G.V., Fiedler, F., Calvo, E.L., Ortiz, E.M., Vasseur, S., Keim, V., Morisset, J., and Iovanna, J.L. 1997. Cloning and expression of the rat p8 cDNA, a new gene activated in pancreas during the acute phase of pancreatitis, pancreatic development, and regeneration, and which promotes cellular growth. *J Biol Chem* 272:32360-32369.

2. Goruppi, S., and Iovanna, J.L. 2010. Stress-inducible protein p8 is involved in several physiological and pathological processes. *J Biol Chem* 285:1577-1581.

3. Cano, C.E., Hamidi, T., Sandi, M.J., and Iovanna, J.L. 2011. Nupr1: the Swiss-knife of cancer. *J Cell Physiol* 226:1439-1443.

4. Garcia-Montero, A., Vasseur, S., Mallo, G.V., Soubeyran, P., Dagorn, J.C., and Iovanna, J.L. 2001. Expression of the stress-induced p8 mRNA is transiently activated after culture medium change. *Eur J Cell Biol* 80:720-725.

5. Encinar, J.A., Mallo, G.V., Mizyrycki, C., Giono, L., Gonzalez-Ros, J.M., Rico, M., Canepa, E., Moreno, S., Neira, J.L., and Iovanna, J.L. 2001. Human p8 is a HMG-I/Y-like protein with DNA binding activity enhanced by phosphorylation. *J Biol Chem* 276:2742-2751.

6. Grasso, D., Garcia, M.N., Hamidi, T., Cano, C., Calvo, E., Lomberk, G., Urrutia, R., and Iovanna, J.L. 2014. Genetic inactivation of the pancreatitis-inducible gene Nupr1 impairs PanIN formation by modulating Kras(G12D)-induced senescence. *Cell Death Differ* 21:1633-1641.

7. Hamidi, T., Algul, H., Cano, C.E., Sandi, M.J., Molejon, M.I., Riemann, M., Calvo, E.L., Lomberk, G., Dagorn, J.C., Weih, F., et al. 2012. Nuclear protein 1 promotes pancreatic cancer development and protects cells from stress by inhibiting apoptosis. *J Clin Invest* 122:2092-2103.

8. Malicet, C., Dagorn, J.C., Neira, J.L., and Iovanna, J.L. 2006. p8 and prothymosin alpha: unity is strength. *Cell Cycle* 5:829-830.

9. Malicet, C., Giroux, V., Vasseur, S., Dagorn, J.C., Neira, J.L., and Iovanna, J.L. 2006. Regulation of apoptosis by the p8/prothymosin alpha complex. *Proc Natl Acad Sci U S A* 103:2671-2676.

10. Sandi, M.J., Hamidi, T., Malicet, C., Cano, C., Loncle, C., Pierres, A., Dagorn, J.C., and Iovanna, J.L. 2011. p8 expression controls pancreatic cancer cell migration, invasion, adhesion, and tumorigenesis. *J Cell Physiol* 226:3442-3451.

11. Ree, A.H., Pacheco, M.M., Tvermyr, M., Fodstad, O., and Brentani, M.M. 2000. Expression of a novel factor, com1, in early tumor progression of breast cancer. *Clin Cancer Res* 6:1778-1783.

12. Gironella, M., Malicet, C., Cano, C., Sandi, M.J., Hamidi, T., Tauil, R.M., Baston, M., Valaco, P., Moreno, S., Lopez, F., et al. 2009. p8/nupr1 regulates DNA-repair activity after double-strand gamma irradiation-induced DNA damage. *J Cell Physiol* 221:594-602.

13. Cano, C.E., Hamidi, T., Garcia, M.N., Grasso, D., Loncle, C., Garcia, S., Calvo, E., Lomberk, G., Dusetti, N., Bartholin, L., et al. 2014. Genetic inactivation of Nupr1 acts as a dominant suppressor event in a two-hit model of pancreatic carcinogenesis. *Gut* 63:984-995.

14. Giroux, V., Malicet, C., Barthet, M., Gironella, M., Archange, C., Dagorn, J.C., Vasseur, S., and Iovanna, J.L. 2006. p8 is a new target of gemcitabine in pancreatic cancer cells. *Clin Cancer Res* 12:235-241.

15. Tang, K., Zhang, Z., Bai, Z., Ma, X., Guo, W., and Wang, Y. 2011. Enhancement of gemcitabine sensitivity in pancreatic cancer by co-regulation of dCK and p8 expression. *Oncol Rep* 25:963-970.

16. Palam, L.R., Gore, J., Craven, K.E., Wilson, J.L., and Korc, M. 2015. Integrated stress response is critical for gemcitabine resistance in pancreatic ductal adenocarcinoma. *Cell Death Dis* 6:e1913.

17. Vasseur, S., Hoffmeister, A., Garcia, S., Bagnis, C., Dagorn, J.C., and Iovanna, J.L. 2002. p8 is critical for tumour development induced by rasV12 mutated protein and E1A oncogene. *EMBO Rep* 3:165-170.

18. Emma, M.R., Iovanna, J.L., Bachvarov, D., Puleio, R., Loria, G.R., Augello, G., Candido, S., Libra, M., Gulino, A., Cancila, V., et al. 2016. NUPR1, a new target in liver cancer: implication in controlling cell growth, migration, invasion and sorafenib resistance. *Cell Death Dis* 7:e2269.

19. Guo, X., Wang, W., Hu, J., Feng, K., Pan, Y., Zhang, L., and Feng, Y. 2012. Lentivirus-mediated RNAi knockdown of NUPR1 inhibits human nonsmall cell lung cancer growth in vitro and in vivo. *Anat Rec (Hoboken)* 295:2114-2121.

20. Kim, K.S., Jin, D.I., Yoon, S., Baek, S.Y., Kim, B.S., and Oh, S.O. 2012. Expression and roles of NUPR1 in cholangiocarcinoma cells. *Anat Cell Biol* 45:17-25.

21. Li, J., Ren, S., Liu, Y., Lian, Z., Dong, B., Yao, Y., and Xu, Y. 2017. Knockdown of NUPR1 inhibits the proliferation of glioblastoma cells via ERK1/2, p38 MAPK and caspase-3. *J Neurooncol* 132:15-26.

22. Zeng, C., Yi, B., Li, X., and Chen, J. 2017. [Knockdown of nuclear protein 1 (NUPR1) gene inhibits proliferation and promotes apoptosis of human multiple myeloma U266 cells]. *Xi Bao Yu Fen Zi Mian Yi Xue Za Zhi* 33:1240-1246.

23. Zeng, C., Li, X., Li, A., Yi, B., Peng, X., Huang, X., and Chen, J. 2018. Knockdown of NUPR1 inhibits the growth of U266 and RPMI8226 multiple myeloma cell lines via activating PTEN and caspase activationdependent apoptosis. *Oncol Rep*.

24. Zeng, C., Li, X., Li, A., Yi, B., Peng, X., Huang, X., and Chen, J. 2018. Knockdown of NUPR1 inhibits the growth of U266 and RPMI8226 multiple myeloma cell lines via activating PTEN and caspase activationdependent apoptosis. *Oncol Rep* 40:1487-1494.

25. Zhou, C., Xu, J., Lin, J., Lin, R., Chen, K., Kong, J., and Shui, X. 2018. Long non-coding RNA FEZF1-AS1 promotes osteosarcoma progression by regulating miR-4443/NUPR1 axis. *Oncol Res*.

26. Aguado-Llera, D., Hamidi, T., Domenech, R., Pantoja-Uceda, D., Gironella, M., Santoro, J., Velazquez-Campoy, A., Neira, J.L., and Iovanna, J.L. 2013. Deciphering the binding between Nupr1 and MSL1 and their DNA-repairing activity. *PLoS One* 8:e78101.

27. Neira, J.L., Rizzuti, B., and Iovanna, J.L. 2016. Determinants of the pKa values of ionizable residues in an intrinsically disordered protein. *Arch Biochem Biophys* 598:18-27.

28. Santofimia-Castano, P., Rizzuti, B., Pey, A.L., Soubeyran, P., Vidal, M., Urrutia, R., Iovanna, J.L., and Neira, J.L. 2017. Intrinsically disordered chromatin protein NUPR1 binds to the C-terminal region of Polycomb RING1B. *Proc Natl Acad Sci U S A*.

29. Santofimia-Castano, P., Rizzuti, B., Abian, O., Velazquez-Campoy, A., Iovanna, J.L., and Neira, J.L. 2018. Amphipathic helical peptides hamper protein-protein interactions of the intrinsically disordered chromatin nuclear protein 1 (NUPR1). *Biochim Biophys Acta Gen Subj* 1862:1283-1295.

30. Neira, J.L., Bintz, J., Arruebo, M., Rizzuti, B., Bonacci, T., Vega, S., Lanas, A., Velazquez-Campoy, A., Iovanna, J.L., and Abian, O. 2017. Identification of a Drug Targeting an Intrinsically Disordered Protein Involved in Pancreatic Adenocarcinoma. *Sci Rep* 7:39732.

31. Velazquez-Campoy, A., Sancho, J., Abian, O., and Vega, S. 2016. Biophysical Screening for Identifying Pharmacological Chaperones and Inhibitors Against Conformational and Infectious Diseases. *Curr Drug Targets* 17:1492-1505.

32. Dickman, K.G., and Mandel, L.J. 1990. Differential effects of respiratory inhibitors on glycolysis in proximal tubules. *Am J Physiol* 258:F1608-1615.

33. Nagdas, S., and Kashatus, D.F. 2017. The Interplay between Oncogenic Signaling Networks and Mitochondrial Dynamics. *Antioxidants (Basel)* 6.

34. Santofimia-Castano, P., Lan, W., Bintz, J., Gayet, O., Carrier, A., Lomberk, G., Neira, J.L., Gonzalez, A., Urrutia, R., Soubeyran, P., et al. 2018. Inactivation of NUPR1 promotes cell death by coupling ER-stress responses with necrosis. *Sci Rep* 8:16999.

35. Koch, K., Mansi, K., Haynes, E., Adams, C.E., Sampson, S., and Furtado, V.A. 2014. Trifluoperazine versus placebo for schizophrenia. *Cochrane Database Syst Rev*:CD010226.

36. Pulkoski-Gross, A., Li, J., Zheng, C., Li, Y., Ouyang, N., Rigas, B., Zucker, S., and Cao, J. 2015. Repurposing the antipsychotic trifluoperazine as an antimetastasis agent. *Mol Pharmacol* 87:501-512.

37. Yeh, C.T., Wu, A.T., Chang, P.M., Chen, K.Y., Yang, C.N., Yang, S.C., Ho, C.C., Chen, C.C., Kuo, Y.L., Lee, P.Y., et al. 2012. Trifluoperazine, an antipsychotic agent, inhibits cancer stem cell growth and overcomes drug resistance of lung cancer. *Am J Respir Crit Care Med* 186:1180-1188.

38. Pinheiro, T., Otrocka, M., Seashore-Ludlow, B., Rraklli, V., Holmberg, J., Forsberg-Nilsson, K., Simon, A., and Kirkham, M. 2017. A chemical screen identifies trifluoperazine as an inhibitor of glioblastoma growth. *Biochem Biophys Res Commun* 494:477-483.

39. Zhelev, Z., Ohba, H., Bakalova, R., Hadjimitova, V., Ishikawa, M., Shinohara, Y., and Baba, Y. 2004. Phenothiazines suppress proliferation and induce apoptosis in cultured leukemic cells without any influence on the viability of normal lymphocytes. Phenothiazines and leukemia. *Cancer Chemother Pharmacol* 53:267-275.

40. Wen, Y., Zhang, Y., Li, J., Luo, F., Huang, Z., and Liu, K. 2018. Low concentration trifluoperazine promotes proliferation and reduces calcium-dependent apoptosis in glioma cells. *Sci Rep* 8:1147.

41. Ruan, H., Sun, Q., Zhang, W., Liu, Y., and Lai, L. 2018. Targeting intrinsically disordered proteins at the edge of chaos. *Drug Discov Today*.

42. Trivedi, R., and Mishra, D.P. 2015. Trailing TRAIL Resistance: Novel Targets for TRAIL Sensitization in Cancer Cells. *Front Oncol* 5:69.

43. Hess, B., Kutzner, C., van der Spoel, D., and Lindahl, E. 2008. GROMACS 4: Algorithms for Highly Efficient, Load-Balanced, and Scalable Molecular Simulation. *J Chem Theory Comput* 4:435-447.

44. Lindorff-Larsen, K., Piana, S., Palmo, K., Maragakis, P., Klepeis, J.L., Dror, R.O., and Shaw, D.E. 2010. Improved side-chain torsion potentials for the Amber ff99SB protein force field. *Proteins* 78:1950-1958.

45. Piana, S., Donchev, A.G., Robustelli, P., and Shaw, D.E. 2015. Water dispersion interactions strongly influence simulated structural properties of disordered protein states. *J Phys Chem B* 119:5113-5123.

46. Trott, O., and Olson, A.J. 2010. AutoDock Vina: improving the speed and accuracy of docking with a new scoring function, efficient optimization, and multithreading. *J Comput Chem* 31:455-461.

47. Wang, J., Wolf, R.M., Caldwell, J.W., Kollman, P.A., and Case, D.A. 2004. Development and testing of a general amber force field. *J Comput Chem* 25:1157-1174.

48. Cavanagh, J.F., Wayne, J., Palmer III, A.G., and Skelton, N.J. 1996. *Protein NMR spectroscopy: principles and practice, 1st Ed.* . San Diego: Academic Press, .

49. Piotto, M., Saudek, V., and Sklenar, V. 1992. Gradient-tailored excitation for single-quantum NMR spectroscopy of aqueous solutions. *J Biomol NMR* 2:661-665.

50. Lomberk, G., Blum, Y., Nicolle, R., Nair, A., Gaonkar, K.S., Marisa, L., Mathison, A., Sun, Z., Yan, H., Elarouci, N., et al. 2018. Distinct epigenetic landscapes underlie the pathobiology of pancreatic cancer subtypes. *Nat Commun* 9:1978.

51. Wu, H., Ying, M., and Hu, X. 2016. Lactic acidosis switches cancer cells from aerobic glycolysis back to dominant oxidative phosphorylation. *Oncotarget* 7:40621-40629.

Table 1: Thermodynamic parameters of the binding reaction, and NUPR1 resonances affected by drug binding (changes in relative intensity with respect to R82)

Compounds	K_d (μM) (=1 /K_a)[a]	Δ*H* (kcal mol^{-1})[a]	n[a]	Resonances[b]
Trifluoperazine	5.2	-1.1	1.0	S1, T3, T8, S9(S22), A10, G16, E18, Y30, A33, H34, G38, G39(G61), G40, G41, G44, A50, N53(S23), T54, S58, G60, E63, T68, S73
ZZW-111	7.5	-1.5	1.1	S1, A2, T3, T8, S9(S22), Q12, G16, E18, H34, Y30, G38,G40, G41,G44,T46, A50, N53(S23), T54, S58, G60, Q71, S73
ZZW-112	11	-1.0	1.0	S1, A2, T3, T8, A10, Q12, G16, E18, S31(S35), H34, G38, G39(G61), G40, G41, G44, T46, A50, N53(S23), T54, S58, G60, E63, T68, Q71, N72, S73
ZZW-115	2.1	-0.4	0.98	A2, T8, S31(S35), H34, N53(S23), H62, E63, G79
ZZW-116	15	-1.2	1.2	T8, S9(S22), A33, H34, G39(G61), G41, G44, H62
ZZW-119	18	-3.4	0.97	T8, Q12, E18, L29, Y30, A33, H34, G38, G44, T68
ZZW-120	7.1	-2.0	1.0	T8, A10, Q12, S31(S35), H34, H62, K65, Q71, G79
ZZW-124	10	-1.2	0.96	A2, G16, H34, G38, G39(G61), G44, N53(S23), G60, H62, E63, T68, Q71, N72, G79

[a] Obtained from ITC measurements.

[b] The colour indicates the changes of the relative intensity of cross-peaks: 0.10 = ΔI< 0.20, 0.20 = ΔI < 0.30, 0.30 = ΔI ≤ 0.40 and ΔI >0.40.

Residues within parenthesis indicate signal overlapping.

Table 2: IC_{50} of TFP-derived compounds on PADC-derived cells

Compounds	IC_{50} (µM)				
	MiaPaCa-2	02.063	LIPC	Foie8b	HN14
Trifluoperazine	9.28	10.12	7.80	8.08	15.90
ZZW-111	3.99	4.63	4.08	5.07	8.84
ZZW-112	8.84	9.85	6.70	9.21	14.44
ZZW-115	1.03	1.18	1.89	3.18	4.52
ZZW-116	8.05	8.90	8.01	8.35	17.95
ZZW-119	3.80	4.03	4.28	4.06	8.62
ZZW-120	9.34	10.94	7.93	9.34	15.57
ZZW-124	8.42	9.27	8.67	9.58	16.36

Figure 1

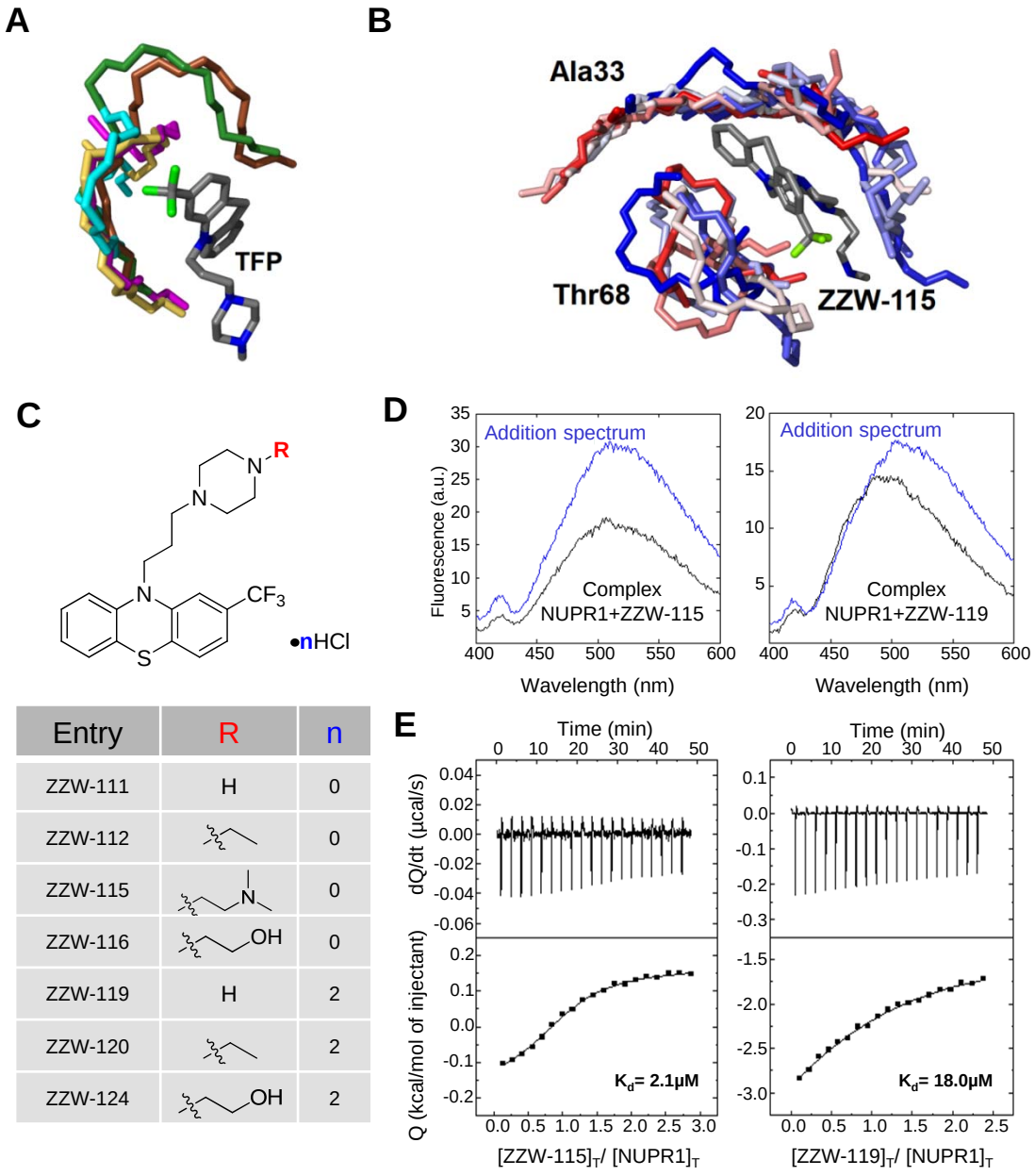

Entry	R	n
ZZW-111	H	0
ZZW-112		0
ZZW-115		0
ZZW-116		0
ZZW-119	H	2
ZZW-120		2
ZZW-124		2

Synthesis of the compounds, and docking and biophysical characterization of NUPR1 to the TFP-derived compounds. (A) Docking of TFP to short fragments of NUPR1 sequence (in different colors), mimicking potential binding locations. The phenothiazine and trifluoromethyl groups of TFP are critical for anchoring, whereas the rest of the structure contributes less. (B) Example of simulation of **ZZW-115** (a single representative structure is shown in gray) in complex with sequence segments of NUPR1 (ensembles are in gradients of color, from red to blue); the labels indicate the central protein residue for each of the two 7-residue fragment. (C) Structure of the synthesized TFP-derived compounds. (D) Fluorescence ANS spectra in the presence or in the absence of **ZZW-115** (left) and **ZZW-119** (right) for the complex between both molecules (black) and for that obtained from the addition of the spectra of both isolated molecules: NUPR1 and the TFP-derived compound (blue). Experiments were performed in 20 mM sodium phosphate pH 7.0, at 25 °C. (E) Calorimetric titrations corresponding to the interaction of **ZZW-115** (left) and **ZZW-119** (right) with NUPR1. Thermograms (thermal power as a function of time) are shown in upper panels, and binding isotherms (ligand-normalized heat effects as a function of molar ratio) are shown in lower panels. Experiments were performed at 25°C in sodium phosphate 20 mM, pH 7, 2% DMSO, with 20 µM NUPR1 in the calorimetric cell and 200 µM compound in the titrating syringe, using an Auto-iTC200 instrument (MicroCal-Malvern Panalytical).

Figure 2

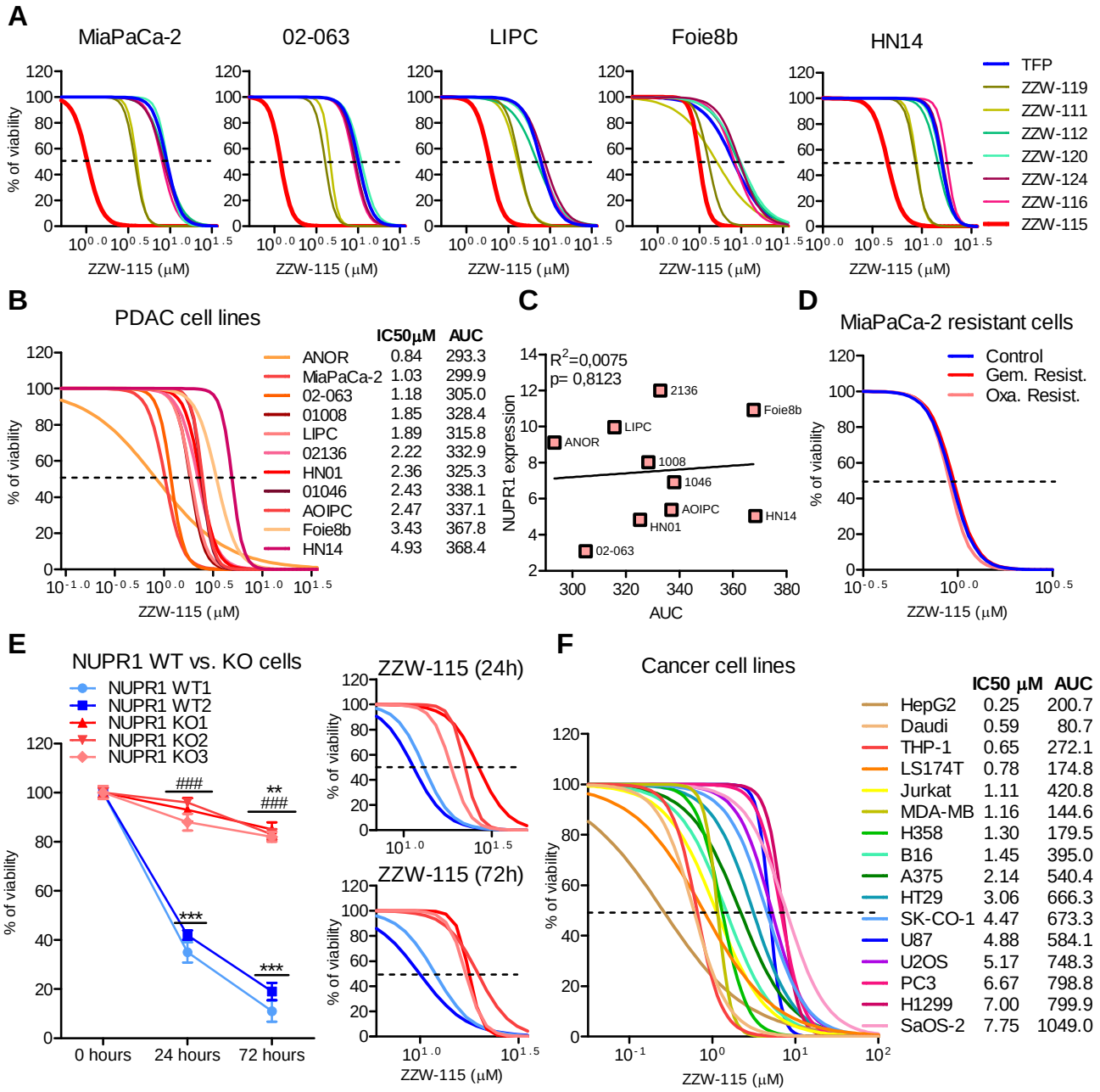

TFP-derived compounds have antitumoral effect due to NUPR1 inhibition. (A) Viability upon a 72 h treatment with TFP-derived compounds of pancreatic cancer cells MiaPaCa2, 02-063, LIPC, Foie8b and HN14. (B) Viability of a panel of 11 additional pancreatic cancer cells upon a 72 h treatment with **ZZW-115**. (C) NUPR1 expression values by RNA-seq are plotted against AUC. Data were statistically analyzed by simple linear regression and R^2 and p values calculated. (D) Chemograms assays to test the sensitivity of the MiaPaCa-2 resistant cells to gemcitabine or oxaliplatin after **ZZW-115** treatment. (E) Viability of 2 NUPR1 WT clones and 3 NUPR1 KO clones PDAC cells upon a 24 or 72 h treatment with 15 µM **ZZW-115**, or at increasing concentrations. (F) Viability of cell lines U87, A375, U2OS, SaOS-2, HT29, SK-CO-1, LS174T, H1299 and H358, HepG2, PC3, THP-1, Daudi, Jurkat and MDA-MB-231 at increasing concentrations of **ZZW-115**. AUC: area under the curve obtained from integration. Statistical significance: *p < 0.05, **p < 0.01, and ***p < 0.001, compared with 0 h treatment; #p < 0.05, ##p < 0.01, and ###p < 0.001 compared with NUPR1 WT clones (2-way ANOVA, Bonferroni post-hoc test). Data represent mean ± SEM, n=3 (with technical triplicates).

Figure 3

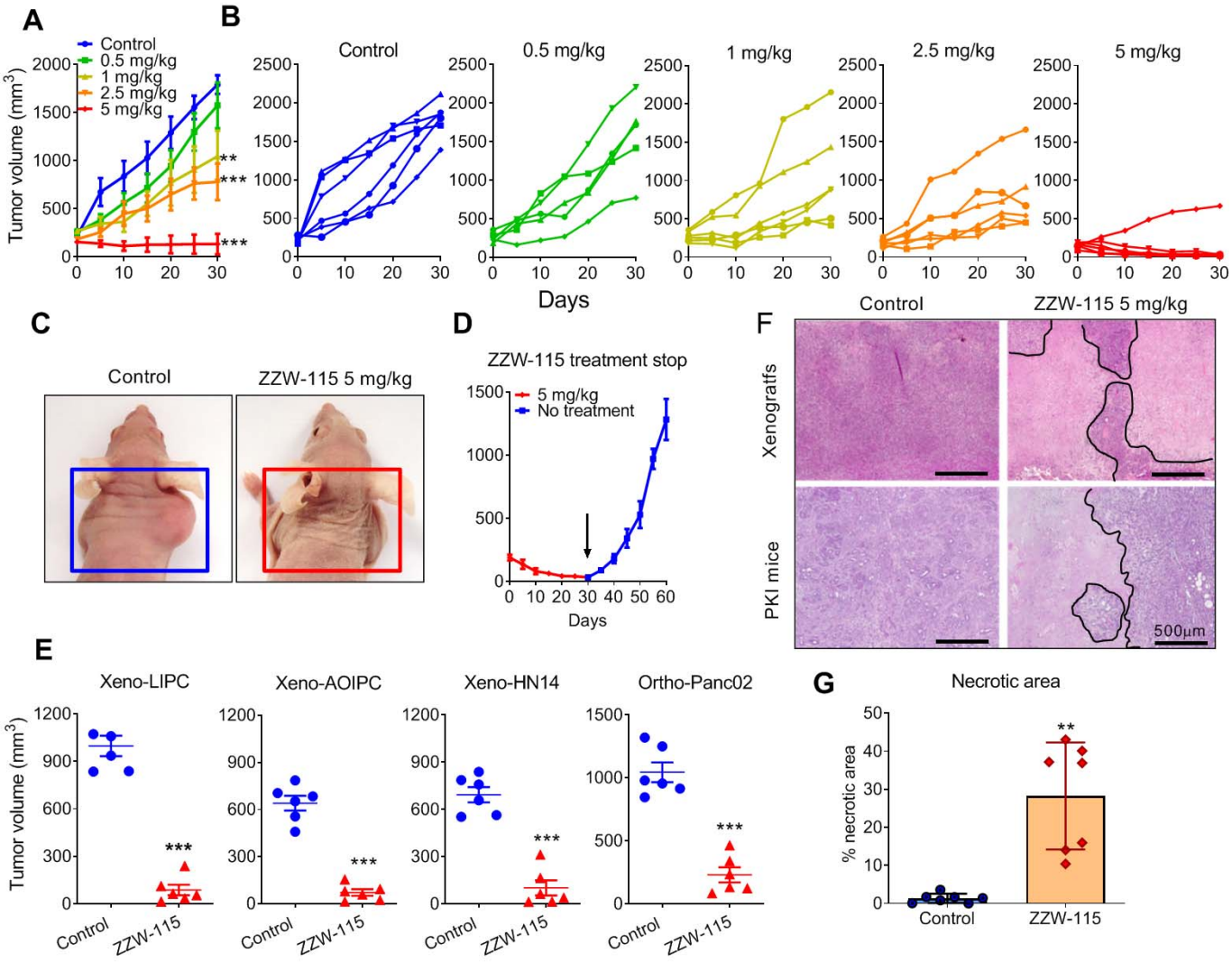

ZZW-115 has strong antitumoral effect in vivo. NMRI-Foxn1nu/Foxn1nu mice (nude mice) xenografted with MiaPaCa-2 cells were separated into five groups of six mice and treated daily during 30 days with 0.5% DMSO in physiologic serum (control group), or either 5 , 2.5, 1.0 or 0.5 mg/kg of **ZZW-115** compound. Tumor volume was measured every 5 days. Mean of the volume of each treatment (A) and individual volume of each mouse (B) are shown. For each treatment, statistical significance is *p < 0.05, **p < 0.01, and ***p < 0.001 (1-way ANOVA, Tukey's post-hoc test). (C) Representative pictures of mice from control and 5 mg/kg **ZZW-115**-treatment groups. (D) Tumor volume of five mice treated with 5 mg/kg of **ZZW-115** measured after additional 30 days without treatment; the arrow indicates the day the treatment was stopped. Student's 2-tailed unpaired t test (E) Tumor volume of nude mice xenografted with PDAC cells or C57BL/6 mice orthotopically implanted with Panc02 cells were treated with 5 mg/kg of **ZZW-115** or vehicle. Tumor volume correspond to after 30 days of treatment (n=6). (F) Representative pictures of histologic sections of the tumor xenografts or tumors from PDX1-Cre;$Kras^{G12D}$;$Ink4a^{flox/flox}$, PKI mice (both from control or 5 mg/kg **ZZW-115**-treated mice). (G) Necrotic area in PKI mice mice calculated for n=9 mice. For each treatment, statistical significance is *p < 0.05, **p < 0.01, and ***p < 0.001 (Student's 2-tailed unpaired t test).

Figure 4

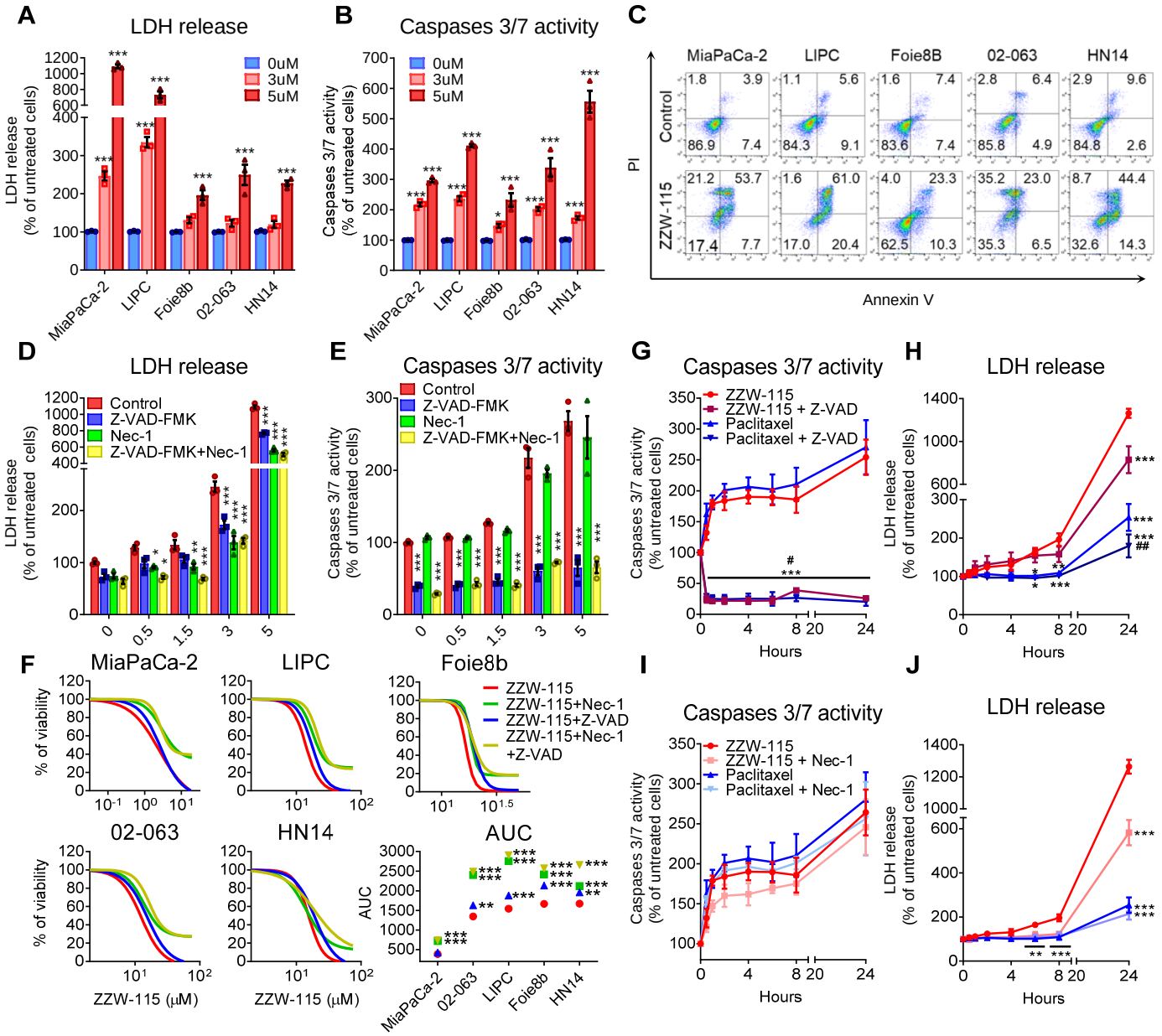

ZZW-115 induces cell death by necrosis and apoptosis in vitro. A panel of pancreatic cancer cell lines was incubated at 3 or 5 µM of **ZZW-115** during 24 h and (A) LDH release and (B) Caspase 3/7 activity were measured. Statistical significance is *p < 0.05, **p < 0.01 and ***p < 0.001 compared to untreated group (2-way ANOVA, Bonferroni post-hoc test). (C) Flow cytometry analysis of annexin-V/PI staining following 24 h of treatment with 5 µM of **ZZW-115**, a representative experiment of the dot plot profile of cells is shown (n=3). MiaPaCa-2 cells were incubated from 0.5 to 5 µM of **ZZW-115** in the presence or not of Z-VAD-FMK (20 µM) or/and Nec-1 (40 µM) during 24 h, and (D) LDH release and (E) Caspase 3/7 activity were measured. Statistical significance is *p < 0.05, **p < 0.01 and ***p < 0.001 compared to control group (2-way ANOVA, Bonferroni post-hoc test). (F) Chemograms assays were done on pancreatic cancer cell lines with increasing concentrations of **ZZW-115** and in the presence or absence of Z-VAD-FMK (20 µM) or/and Nec-1 (40 µM) during 24 h. AUC: area under the curve calculated by integration. Statistical significance is *p < 0.05, **p < 0.01 and ***p < 0.001 compared to **ZZW-115** treated cells (2-way ANOVA, Bonferroni post-hoc test). MiaPaCa-2 cells were incubated at 5 µM of **ZZW-115** compound or 8 nM of paclitaxel in the presence or in the absence of Z-VAD-FMK (20 µM) and (G) Caspase 3/7 activity and (H) LDH release were measured. MiaPaCa-2 cells were incubated at 5 µM of **ZZW-115** or 8 nM of paclitaxel in the presence or absence of Nec-1 (40 µM) and (I) Caspase 3/7 activity, and (J) LDH release were measured. Statistical significance is *p < 0.05, **p < 0.01 and ***p < 0.001 compared to **ZZW-115** treated cells; #p < 0.05, ##p < 0.01, and ###p < 0.001 compared with Paclitaxel treated cells (2-way ANOVA, Bonferroni post-hoc test). Data represent mean ± SEM, n=3.

Figure 5

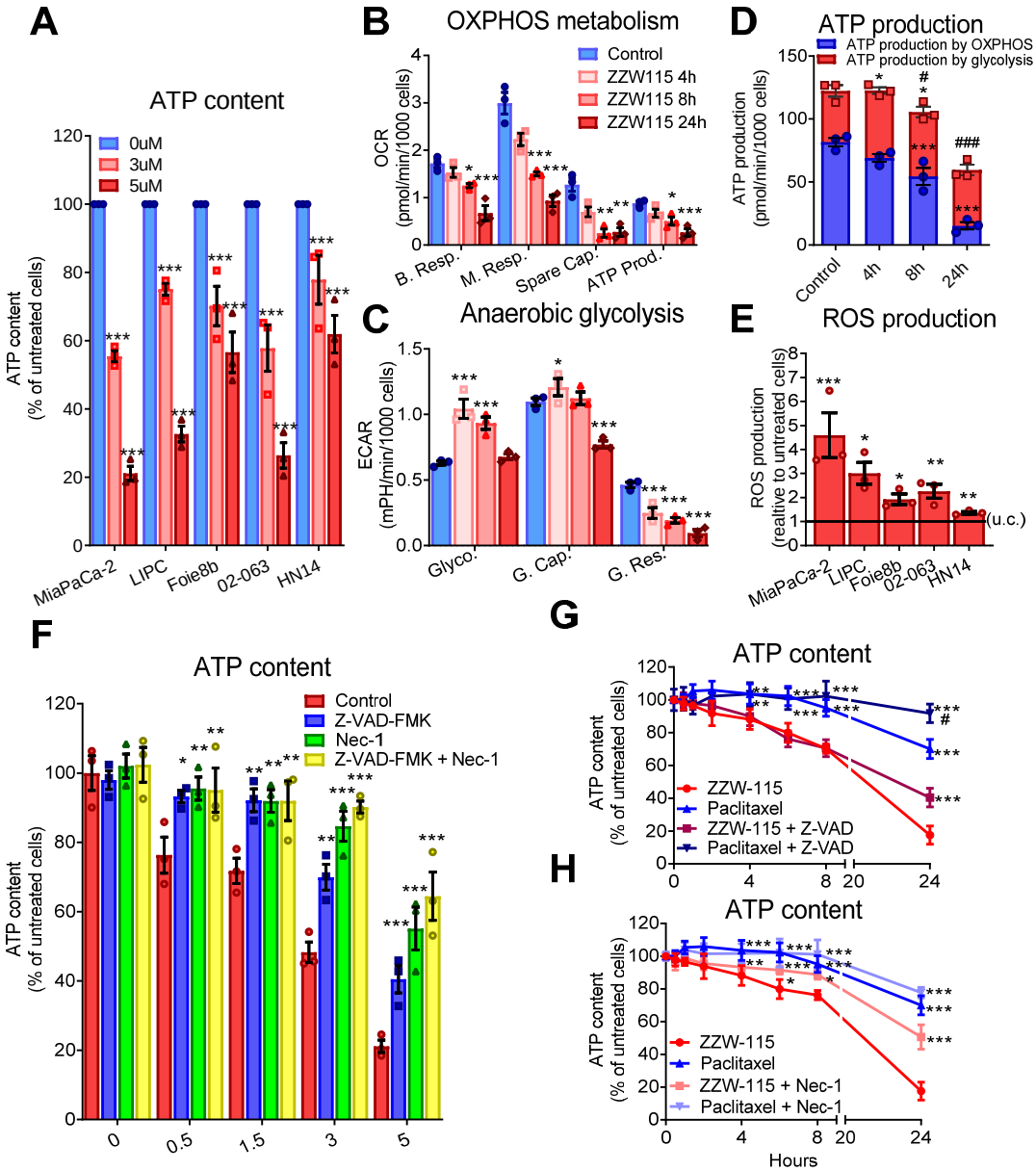

ZZW-115 treatment induces a decrease in ATP production and ROS overproduction. (A) ATP content measured in a panel of pancreatic cancer cell lines incubated at 3 or 5 µM of **ZZW-115** during 24 h. (B) OXPHOS metabolism, reflected by oxygen consumption rate (OCR) levels for Basal respiration, Maximal respiration, Spare capacity and ATP production and (C) Anaerobic glycolytic metabolism reflected by extracellular acidification rate (ECAR) levels for Glycolysis, Glycolytic capacity and Glycolysis reserve were measured in MiaPaCa-2 cells treated with 3 µM of **ZZW-115** compound during 4, 8 or 24 h. (D) ATP production by OXPHOS and anaerobic glycolysis were determined, in MiaPaCa-2 cells treated with 3 µM of **ZZW-115** during 4, 8 or 24 h. Statistical significance: *p < 0.05, **p < 0.01 and ***p < 0.001 for OXPHOS or glycolysis compared to control cells; #p < 0.05, ##p < 0.01, and ###p < 0.001 for total ATP compared to control cells (2-way ANOVA, Bonferroni post-hoc test). (E) ROS production was detected using MitoSOX Red by flow cytometry analysis on a panel of pancreatic cancer cell lines incubated with **ZZW-115** at 3 µM. Statistical significance: *p < 0.05, **p < 0.01 and ***p < 0.001 compared to control cells (Student's 2-tailed unpaired t test). (F) MiaPaCa-2 cells were incubated at a **ZZW-115** concentrations range of 0.5 to 5 µM in the presence or in the absence of Z-VAD-FMK (20 µM) or/and Nec-1 (40 µM) during 24 h, and ATP content was measured. (G and H) MiaPaCa-2 cells were incubated at 5 µM of **ZZW-115** or 8 nM of paclitaxel in the presence or in the absence of Z-VAD-FMK (20 µM) or Nec-1 (40 µM), and ATP content was measured. Statistical significance: *p < 0.05, **p < 0.01 and ***p < 0.001 compared to **ZZW-115** treated cells; #p < 0.05, ##p < 0.01, and ###p < 0.001 compared with Paclitaxel treated cells (2-way ANOVA, Bonferroni post-hoc test). Data represent mean ± SEM, n=3.